GSA Data Repository Item 2016236
Craddock, J.P., Schmitz, M.D., Crowley, J.L., Larocque, J., Pankhurst, R.J., Juda, N., Konstantinou, A., and Storey, B., 2016, Precise U-Pb Zircon Ages and Geochemistry of Jurassic Granites, Ellsworth-Whitmore Terrane, Central Antarctica: GSA Bulletin, doi:10.1130/B31485.1.

APPENDICES

Appendix 1. Detailed Methods

Appendix 2. Geologic map, Pirritt Hills.

Appendix 3. Geologic map, Martin Hills.

Appendix 4. Geologic map, Nash Hills.

Appendix 5. Geologic map, Hart Hills.

Appendix 6. West Antarctic granite geochemistry (non-EWT).

APPENDIX 1: ANALYTICAL METHODS

X-Ray Fluorescence Geochemistry

Samples were split with a vise wedge and only pieces lacking weathered or sawmarked edges were used in XRF analyses. Powders were prepared by further splitting the sample and reducing these pieces to a fine powder in a Spex 8510 shatterbox. The use of pre-contaminated bowls (iron for trace element and tungsten carbide for major element powders) reduced the chance of cross contamination between the samples. Pressed powder pellets were prepared for trace element analyses by mixing 10 g of rock powder with 15 drops of 2% polyvinyl alcohol and pressing the mixture into pellets on a stainless steel mold under a pressure of 6 tonnes. Major element concentrations were determined from fused glass beads that were prepared with dried sample powder that was mixed with lithium metaborate/tetraborate flux. The sample pellets and beads were analyzed using a Phillips PW-2400 X-ray fluorescence spectrometer. Elemental concentrations were determined by comparing X-ray intensities for each element in a sample unknown with those from >40 international reference materials. Trace element concentrations were corrected for matrix effects using the Rh tube Compton K alpha scatter peak ratio method. Details of XRF sample preparation, analyses, analytical precision, and detection limits are provided in Vervoort et al. (2007).

Tracer Isotopes (Sr, Pb, Nd)

For Sm-Nd isotopic analysis, fifty milligram aliquots of sample powder were spiked with a mixed ^{149}Sm-^{150}Nd tracer, dissolved with 5 mL 29M HF + 15M HNO_3 (3:1) in Parr pressure vessels at 200 °C for 72 h, dried and re-dissolved in 5 mL 6M HCl at 120 °C for 24 h. Total dissolutions were dried and re-dissolved in 5 mL 1M HCl + 0.1M HF at 120 °C overnight. Bulk rare earth elements were separated by standard dilute HCl and HNO_3 based cation exchange chemistry (Richard et al., on 6mm i.d. × 20 cm columns of AG-50W-X8 resin, (H^+ form, 200–400 mesh); Sm and Nd were separated by reverse phase HDEHP chromatography on 4 mm i.d. × 10 cm columns of Eichrom Ln-spec resin, 50–100 mesh. Sm and Nd isotopes were measured on an IsotopX Isoprobe-T in static and dynamic Faraday modes, respectively. Instrumental mass fractionation of Sm and Nd isotopes was corrected with an exponential law relative to ^{146}Nd/^{144}Nd = 0.7219 and ^{152}Sm/^{147}Sm = 1.783. The ^{143}Nd/^{144}Nd ratio is reported as spike-stripped and bias-corrected relative to the accepted value of JNdi-1 standard (0.512115; Tanaka et al., 2000).

For Rb-Sr isotopic analyses, we selected apatite as the preferred phase from which to extract initial Sr isotopic compositions, based upon its relatively low Rb/Sr and lack of secondary alteration. From 1 to 5 mg of apatite were spiked with a mixed ^{87}Rb-^{84}Sr tracer, dissolved with 1 mL 15M HNO_3 in Savillex PFA beakers at 150 °C for 60 h, dried and redissolved in 5 mL 6M HCl at 150 °C for 16 h. The resulting clear solution was dried and redissolved in 1 mL 3.5M HNO_3 at 150 °C overnight. Sr was separated via an ion exchange column procedure in 3.5M HNO_3 media using 50 µl of Sr-spec crown ether resin (Eichrom); Rb was collected from the initial washes from this column, and further purified by ion exchange in 0.6M HCl on 6mm i.d. × 10 cm columns of AG-50W-X8 resin (H^+ form, 200–400 mesh). Rb and Sr were loaded in 0.1N H_3PO_4 along with a tantalum oxide emitter solution (R. Creaser, pers. comm.) on single degassed Re filaments, and their isotope ratios measured on the Isoprobe-T in the Boise State University Isotope Geology Laboratory. The ^{87}Rb/^{85}Rb ratio was measured

in static Faraday mode; a mass bias correction was estimated by external analysis of natural Rb standards. Sr isotope ratios were analyzed in dynamic mode, fractionation corrected with an exponential law relative to $^{86}Sr/^{88}Sr = 0.1194$, and are reported as spike-stripped and bias corrected relative to the accepted value of the NBS-987 standard (0.710248).

For Pb isotopic analyses, up to 200 mg of potassium feldspar were isolated by selective density separation in lithium polytungstate (Geoliquids), followed by handpicking. Separates were progressively leached following methods modified from Housh and Bowring (1991). All leaching was accomplished in savillex Teflon beakers on a hot plate at 50 °C, and each leach step was followed by rinsing with two aliquots of 500 µl high-purity H_2O which was subsequently added to the leachate. After leaching with 500 µl 7 M HNO_3 and 6 M HCl for 15 min each, separates were subjected to five sequential treatments of 500 µl of 5% HF for 10 min each. All HF leachates were dried and re-dissolved in 0.5 M HBr for separation of Pb by anion exchange chemistry. Total procedural blanks were <20 pg, and thus represent a negligible contribution to the sample Pb.

Purified Pb elutions were dried with 2 µl of 0.05 N H_3PO_4, and then loaded on single degassed Re filaments with 2 µl of a silica-gel/phosphoric acid mixture (Gerstenberger and Haase, 1997). Pb isotope ratios were measured in static Faraday mode for 200 ratios over a restricted and reproducible range in temperature, with ^{208}Pb ion beams ranging from 1 to 4V. Ratios were corrected for instrumental mass fractionation of 0.10 ± 0.03%/a.m.u., as estimated by repeated analyses of NBS 981 and 982 over the same temperature range. Successive HF leaches yielded progressively less radiogenic isotopic compositions, which usually achieved a plateau by the fourth and fifth leach steps; the least radiogenic isotopic composition for each feldspar separate is reported in Table 2, and is assumed to closely approach the initial isotopic composition of the magma from which the feldspar crystallized.

U-Pb Geochronology Methods (ID-TIMS)

Zircons were extracted from crushed rock samples using standard density and magnetic separation methods, mounted in epoxy, polished until the centers were exposed, and imaged with a scanning electron microscope using a cathodo-luminescence detector (CL) at Carleton College, MN. The CL images were used to guide the selection of grains for dating in the Boise State University Isotope Geology Laboratory. Analyses were exclusively from single grains extracted from the mounts. All imaged grains have sector and oscillatory zoning that is typical of zircon crystallized from granitic magmas; grains with obvious inherited components (as identified by contrasts in CL or zoning truncations) were avoided.

Zircon crystals were subjected to a modified version of the chemical abrasion method of Mattinson (2005), reflecting a preference to prepare and analyze carefully selected single crystals. Zircons extracted from mounts were placed in a muffle furnace at 900 °C for 60 h in quartz beakers, transferred to individual 3 ml Teflon PFA beakers with ultrapure H_2O, and then loaded into 300 µl Teflon PFA dissolution microcapsules. Fifteen microcapsules were placed in a large-capacity Parr vessel, and the crystals partially dissolved in 120 µl of 29 M HF for 10–12 h at 180 °C. The contents of each microcapsule were returned to 3 ml Teflon PFA beakers, the HF removed and the residual grains rinsed in ultrapure H_2O, immersed in 3.5 M HNO_3, ultrasonically cleaned for an hour, and fluxed on a hotplate at 80 °C for an hour. The HNO_3 was removed and the grains were rinsed several times with ultrapure H_2O before being reloaded into the same 300 µl Teflon PFA dissolution microcapsules (rinsed and fluxed in 6 M HCl during

crystal sonication and washing) and spiked with the Boise State University mixed ^{233}U-^{235}U-^{205}Pb tracer solution (which has been calibrated against EARTHTIME gravimetric standards). The grains were dissolved in Parr vessels in 120 µl of 29 M HF with a trace of 3.5 M HNO_3 at 220 °C for 48 h, dried to fluorides, and then re-dissolved in 6 M HCl at 180 °C overnight. U and Pb were separated from the zircon matrix using an HCl-based anion-exchange chromatographic procedure (Krogh, 1973), eluted together and dried with 2 µl of 0.05 N H_3PO_4.

Pb and U were loaded on a single outgassed Re filament in 2 µl of a silica-gel/phosphoric acid mixture (Gerstenberger and Haase, 1997), and U and Pb isotopic measurements made on an IsotopX GV Isoprobe-T multicollector thermal ionization mass spectrometer equipped with an ion-counting Daly detector. Pb isotopes were measured by peak-jumping all isotopes on the Daly detector for 100–150 cycles, and corrected for 0.18 ± 0.04%/a.m.u. (atomic mass unit) mass fractionation. Transitory isobaric interferences due to high-molecular weight organics, particularly on ^{204}Pb and ^{207}Pb, disappeared within ~30 cycles, while ionization efficiency averaged 10^4 cps/pg of each Pb isotope. Linearity (to $\geq 1.4 \times 10^6$ cps) and the associated dead-time correction of the Daly detector were monitored by repeated analyses of NBS982, and have been constant since installation. Uranium was analyzed as UO_2^+ ions in static Faraday mode with 10^{11} ohm resistors for 150–200 cycles, and corrected for isobaric interference of $^{233}U^{18}O^{16}O$ on $^{235}U^{16}O^{16}O$ with an $^{18}O/^{16}O$ of 0.00206. Ionization efficiency averaged 20 mV/ng of each U isotope. U mass fractionation was corrected using the known $^{233}U/^{235}U$ ratio of the BSU tracer solution.

U-Pb dates and uncertainties were calculated using the algorithms of Schmitz and Schoene (2007) and the U decay constants Jaffey et al. (1971). $^{206}Pb/^{238}U$ ratios and dates were corrected for initial ^{230}Th disequilibrium using a Th/U[magma] of 3 ± 1, resulting in a systematic increase in the $^{206}Pb/^{238}U$ dates of ~90 k.y. All common Pb in analyses was attributed to laboratory blank and subtracted based on the measured laboratory Pb isotopic composition and associated uncertainty. U blanks were <0.1 pg. Over the course of the experiment, isotopic analyses of the TEMORA 2 zircon standard yielded a weighted mean $^{206}Pb/^{238}U$ age of 417.43 ± 0.06 (n = 11, MSWD = 0.8).

U-Pb Geochronology Methods (SHRIMP)

Some reported ages were determined using a Sensitive High Resolution Ion Microprobe (SHRIMP) at The Australian National University (following Williams, 1998). An epoxy resin mount was prepared from a selection of 50–100 grains, ground half-way through, polished and Au-coated. Internal zoning and the characteristics of individual grains were mapped by a combination of microphotography and cathodoluminescence (CL) imaging. Targets were carefully selected so that clean areas, free of cracks, inclusions and radiation damage could be analyzed, in order to date specific phases of zircon growth—generally the latest igneous phase with concentric oscillatory zoning, although in the case of the Linck Nunataks sample some cores were also targeted. Analysis was carried out with a primary O^- beam and secondary ion beam intensities were measured using an ion-counting detector. Calibration was carried out using chips of laboratory zircon standard SL13 mounted together with the samples and the data were processed using SQUID (Ludwig, 2003).

REFERENCES CITED

Gerstenberger, H., and Haase, G., 1997, A highly effective emitter substance for mass spectrometric Pb isotope ratio determinations: Chemical Geology, v. 136, p. 309–312, doi:10.1016/S0009-2541(96)00033-2.

Housh, T., and Bowring, S.A., 1991, Lead isotopic heterogeneities within alkali feldspars: Implications for the determination of initial lead isotopic compositions: Geochimica et Cosmochimica Acta, v. 55, p. 2309–2316, doi:10.1016/0016-7037(91)90106-F.

Jaffey, A.H., Flynn, K.F., Glendenin, L.E., Bentley, W.C., and Essling, A.M., 1971, Precision measurement of half-lives and specific activities of 235U and 238U: Physical Review C: Nuclear Physics, v. 4, p. 1889–1906, doi:10.1103/PhysRevC.4.1889.

Krogh, T.E., 1973, A low contamination method for the hydrothermal dissolution of zircon and extraction of U and Pb for isotopic age determinations: Geochimica et Cosmochimica Acta, v. 37, p. 485–494, doi:10.1016/0016-7037(73)90213-5.

Ludwig, K.R., 2003, User's Manual for Isoplot 3.00: A Geochronological Toolkit for Microsoft Excel: Berkeley Geochronology Center Special Publication 4, 70 p.

Mattinson, J.M., 2005, Zircon U-Pb chemical abrasion ("CA-TIMS") method: Combined annealing and multi-step partial dissolution analysis for improved precision and accuracy of zircon ages: Chemical Geology, v. 220, p. 47–66, doi:10.1016/j.chemgeo.2005.03.011.

Schmitz, M.D., and Schoene, B., 2007, Derivation of isotope ratios, errors and error correlations for U-Pb geochronology using ^{205}Pb-^{235}U-(^{233}U)-spiked isotope dilution thermal ionization mass spectrometric data: Geochemistry Geophysics Geosystems, v. 8, G3, Q08006, doi:10.1029/2006GC001492.

Tanaka, T., Togashi, S., Kamioka, H., Amakawa, H., Kagami, H., Hamamoto, T., Yuhara, M., Orihashi, Y., Yoneda, S., and Shimizu, H., 2000, JNdi-1: a neodymium isotopic reference in consistency with LaJolla neodymium: Chemical Geology, v. 168, p. 279–281, doi:10.1016/S0009-2541(00)00198-4.

Vervoort, J.D., Wirth, K., Kennedy, B., Sandland, T., and Harpp, K.S., 2007, The magmatic evolution of the Midcontinent Rift: New geochronologic and geochemical evidence from felsic magmatism: Precambrian Research, v. 157, p. 235–268, doi:10.1016/j.precamres.2007.02.019.

Williams, I.S., 1998, U-Th-Pb geochronology by ion microprobe, *in* McKibben, M.A., Shanks, W.C., III, and Ridley, W.I., eds., Applications of Microanalytical Techniques to Understanding Mineralizing Processes: Reviews of Economic Geology, v. 7, p. 1–35.

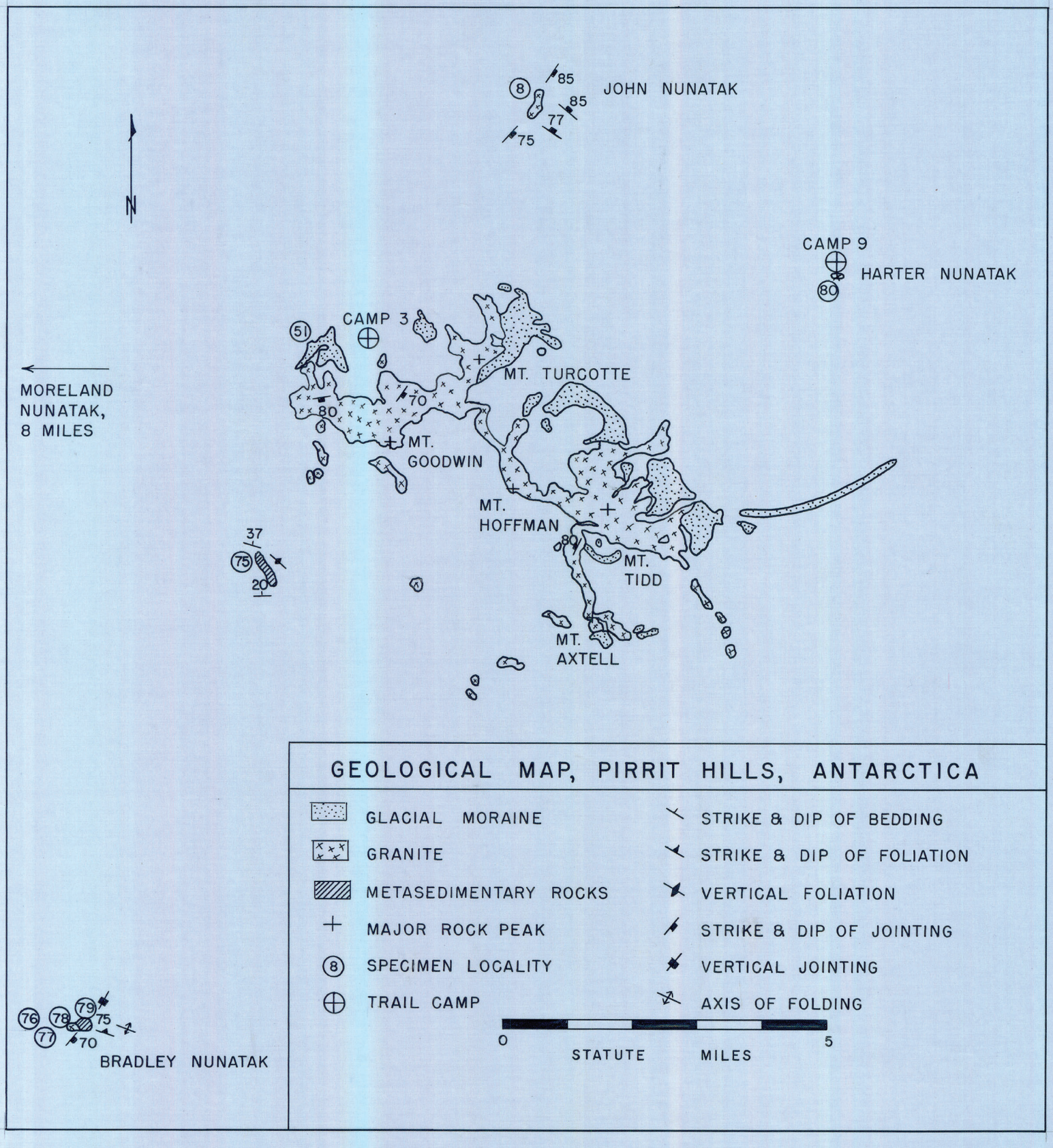

Appendix 2: Geologic map of the Pirrit Hills, central Antarctica.

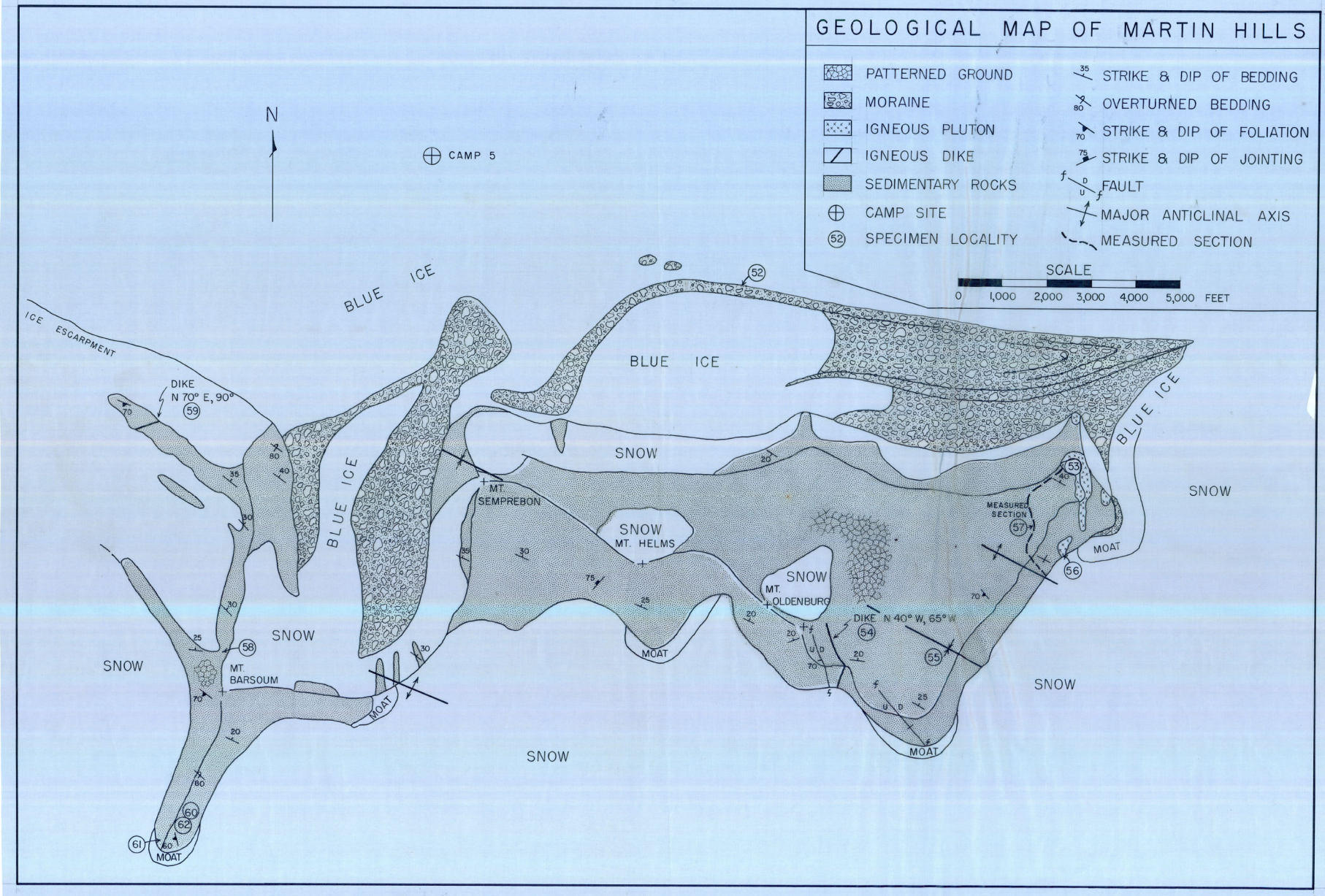

Appendix 3: Geologic map of the Martin Hills, central Antarctica.

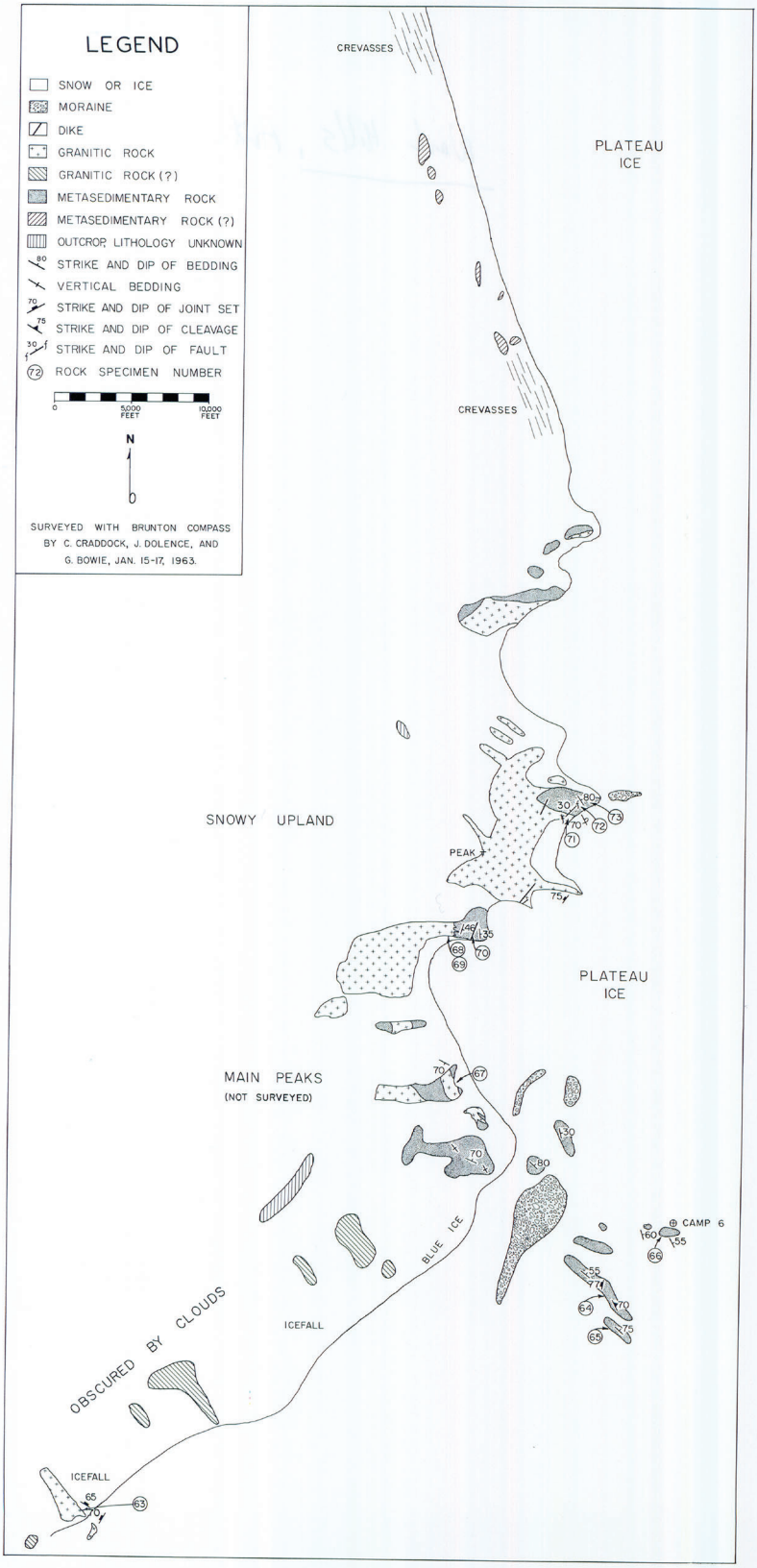

Appendix 4: Geologic map of the Nash Hills, central Antarctica.

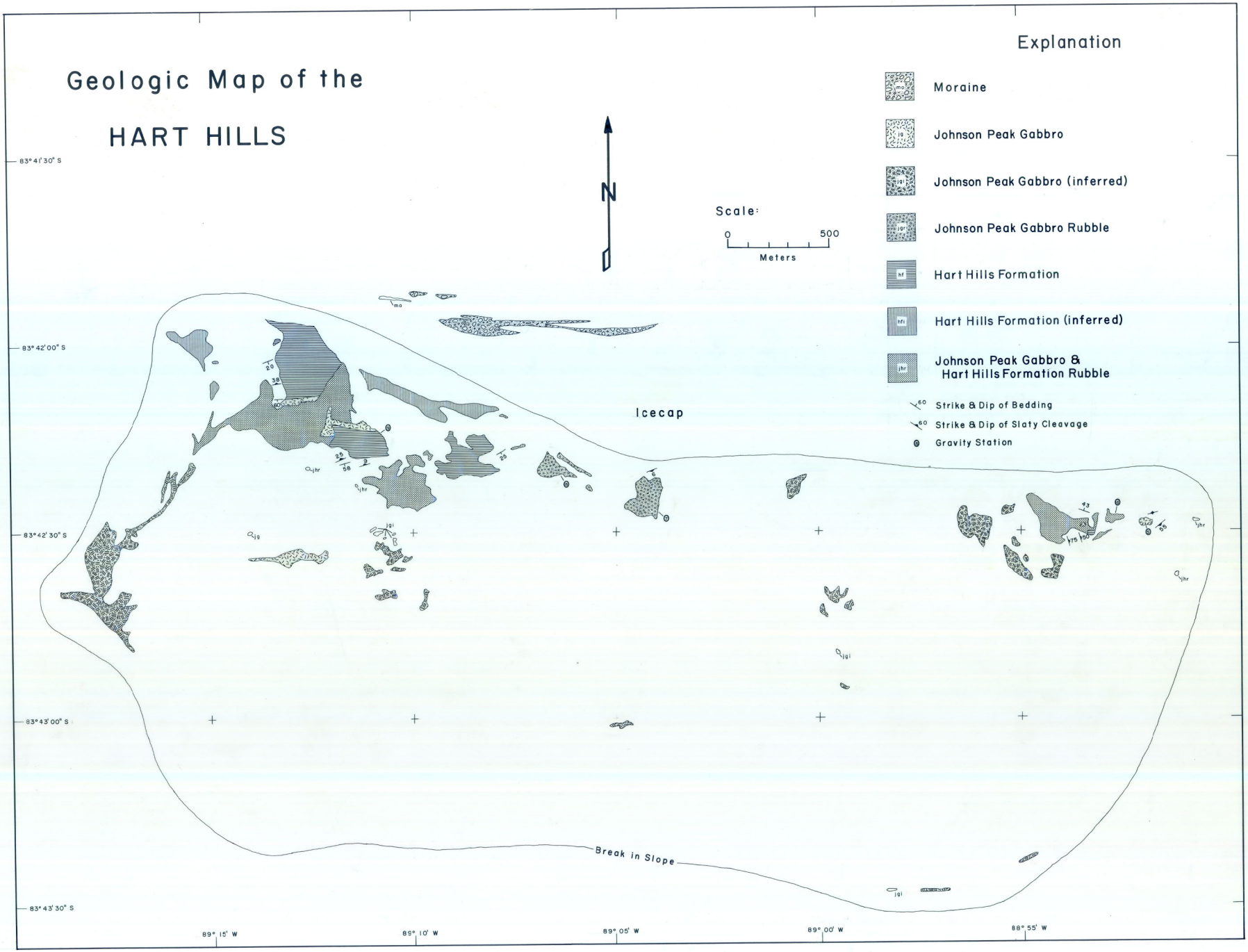

Appendix 5: Geologic map of the Hart Hills, central Antarctica.

Appendix 6 (Supplementary data table): Sr and Nd data from Antarctic Peninsula granitoids.

Sample	Rock type	Locality	Ref.	Age	Rb	Sr	$^{87}Rb/^{86}Sr$	$^{87}Sr/^{86}Sr$	$^{87}Sr/^{86}Sr_i$	Sm	Nd	$^{147}Sm/^{144}Nd$	$^{143}Nd/^{144}Nd$	εNd_i	T_{DM}
Cenozoic (<65 Ma)															
Graham Land															
BR.024.3	DI	Faure Islands	1	48	113	406	0.7999	0.704610	0.704065	7.8	42.8	0.1095	0.512836	4.4	495
BR.024.4	DI	Faure Islands	1	48	36	507	0.2043	0.704210	0.704071	4.0	20.5	0.1186	0.512843	4.5	487
R.008.1	GD	Anchorage Island	1	62	31	443	0.2020	0.704050	0.703872	4.9	21.6	0.1365	0.512866	4.9	453
R.013.4	MD	Anchorage Island	1	62	51	452	0.3273	0.704000	0.703712	5.4	23.7	0.1391	0.512888	5.3	411
North-west Palmer Land															
R.5256.1	GD	Mount Pitman	7	60	103	443	0.6742	0.704968	0.704393	5.5	29.0	0.1147	0.512777	3.3	607
Late Cretaceous (97-65 Ma)															
Graham Land															
R.076.1	DI	Horseshoe Island	1	67	10	778	0.0367	0.704140	0.704105	4.9	20.3	0.1451	0.512807	3.7	574
R.079.1	GA	Horseshoe Island	1	67	11	987	0.0313	0.704180	0.704150	2.9	23.4	0.0746	0.512811	4.4	507
R.080.1	GR	Horseshoe Island	1	67	45	208	0.6196	0.704670	0.704080	7.7	38.4	0.1208	0.512830	4.4	509
BR.138.6	GR	Terra Firma Islands	9	85	85	188	1.3144	0.705960	0.704373	7.6	37.5	0.1230	0.512765	3.3	630
BR.138.13	GA	Terra Firma Islands	9	85	21	654	0.0926	0.704454	0.704342	4.4	19.4	0.1364	0.512752	2.9	668
BR.138.17	DI	Terra Firma Islands	9	85	60	387	0.4444	0.705905	0.705368	5.6	29.1	0.1151	0.512599	0.1	914
R.503.2	GD	Petermann Island	1	93	113	256	1.2776	0.706200	0.704512	7.7	40.4	0.1155	0.512706	2.3	728
BR.132.15	GR	Bourgeois Fjord	9	96	130	113	3.3150	0.710270	0.705748	4.9	26.6	0.1114	0.512545	-0.8	997
R.5860.1	GD	Sellar Glacier	9	96	117	424	0.7953	0.707158	0.706073	2.7	15.9	0.1021	0.512531	-0.9	1010
North-west Palmer Land															
R.5736.1	GD	Scorpio Peaks	7	70	76	570	0.3879	0.704667	0.704281	4.2	24.9	0.1034	0.512821	4.4	511
R.5955.11	GD	Orion Massif	9	70	75	589	0.3694	0.705499	0.705131	4.7	25.2	0.1136	0.512718	2.3	711
R.5501.1	GD	Mount Lepus	9	80	86	150	1.6621	0.707292	0.705403	3.2	22.7	0.0846	0.512660	1.6	784
R.5965.7	GD	Mount Lepus	9	80	80	493	0.4718	0.705913	0.705376	4.9	29.0	0.1030	0.512685	1.9	757
R.5267.1	GD	Goettel Escarpment	9	87	55	496	0.3203	0.706827	0.706431	6.1	30.5	0.1209	0.512531	-1.2	1029
R.2539.2	GD	Taurus Nunataks	9	88	31	935	0.0955	0.706768	0.706648	2.7	14.5	0.1108	0.512479	-2.1	1103
R.5271.1	PO	Goettel Escarpment	9	91	53	691	0.2236	0.705980	0.705691	4.1	21.2	0.1155	0.512605	0.3	903
Early Cretaceous (146-97)															
Graham Land															
BR.125.1	GD	Bourgeois Fjord	9	100	80	469	0.4947	0.706979	0.706276	4.1	23.5	0.1050	0.512452	-2.5	1137
BR.129.1	GR	Bourgeois Fjord	9	100	84	215	1.1323	0.706803	0.705194	3.2	19.7	0.0984	0.512596	0.4	898
R.5552.1	GR	Bristly Peaks	9	98	122	88	4.0131	0.711047	0.705458	5.0	27.0	0.1128	0.512586	0.0	931
R.366.1	GR	Cape Fairweather	1	101	152	61	7.2265	0.715976	0.705605	5.1	26.0	0.1190	0.512566	-0.4	970
R.571.1	GR	Horseshoe Island	1	101	212	12	51.8700	0.779990	0.705508	7.5	37.2	0.1225	0.512548	-0.8	1003
North-west Palmer Land															
R.2414.3	GR	Pegasus Mountains	7	140	84	157	1.5449	0.707309	0.704234	3.9	17.8	0.1329	0.512746	3.2	673
R.2418.4	GD	Pegasus Mountains	7	140	42	287	0.4203	0.705580	0.704743	2.6	12.2	0.1290	0.512625	1.0	880
R.2402.1	GR	Aldebaran Rock	9	140	163	311	1.5216	0.707684	0.704656	7.1	42.6	0.1015	0.512595	0.9	889
R.5902.8	GD	Friedmann Nuns.	7	100	58	638	0.2647	0.706755	0.706379	4.1	21.8	0.1144	0.512449	-2.6	1151
R.2568.2	GD	Sirius Cliffs	9	120	48	753	0.1855	0.707285	0.706968	3.0	19.9	0.0906	0.512431	-2.4	1147
R.5796.4	GD	Cetus Hill	7	120	36	1078	0.0963	0.707003	0.706838	3.2	18.8	0.1023	0.512408	-3.0	1197
R.2556.1	GD	Perseus Crags	7	125	56	642	0.2526	0.707254	0.706805	3.8	18.7	0.1223	0.512437	-2.7	1176
R.5904.7	GD	Puppis Pikes	9	140	76	565	0.3898	0.709361	0.708585	3.6	21.1	0.1034	0.512345	-4.1	1288
R.2585.1	GD	Procyon Peaks	9	140	67	651	0.2994	0.706119	0.705523	6.8	34.2	0.1202	0.512595	0.5	917
R.2784.1	GD	Creswick Gap	8	140	74	287	0.7412	0.706802	0.705327	4.0	23.2	0.1049	0.512547	-0.1	974
R.3204.3	GD	Creswick Gap	8	140	65	569	0.3307	0.706569	0.705911	3.6	19.3	0.1121	0.512510	-1.0	1045
R.3216.2	TO	Burns Bluff	8	140	18	736	0.0712	0.705693	0.705551	2.0	9.4	0.1256	0.512553	-0.4	995
R.3216.3	TO	Burns Bluff	6,8	140	22	612	0.1038	0.705733	0.705526	2.9	14.0	0.1262	0.512539	-0.7	1019
R.5284.1	GD	Renner Peak	9	140	31	910	0.0992	0.706244	0.706046	3.6	20.0	0.1078	0.512509	-0.9	1040
R.5300.3	GA	Auriga Nunataks	9	140	24	452	0.1516	0.707215	0.706913	4.0	11.1	0.2183	0.512536	-2.4	1158
R.5958.1	GD	Wade Point	9	140	30	184	0.4787	0.705202	0.704249	3.8	15.0	0.1523	0.512786	3.7	632

Sample	Rock type	Locality		Age	Rb	Sr	$^{87}Rb/^{86}Sr$	$^{87}Sr/^{86}Sr$	$^{87}Sr/^{86}Sr_i$	Sm	Nd	$^{147}Sm/^{144}Nd$	$^{143}Nd/^{144}Nd$	εNd_i	T_{DM}
R.6314.9	GD	Butler Peaks	7	140	39	573	0.1984	0.706162	0.705767	3.5	19.9	0.1055	0.512479	-1.5	1085
R.6316.4	GD	Butler Peaks	7	140	28	691	0.1166	0.705960	0.705728	3.2	15.3	0.1254	0.512511	-1.2	1063
R.5287.1	DI	Creswick Peaks	7,8	141	77	383	0.5832	0.706879	0.705710	3.3	16.8	0.1170	0.512521	-0.8	1035
R.6057.7	TO	Burns Bluff	6,8	141	31	153	0.5777	0.705836	0.704678	4.3	18.5	0.1394	0.512781	3.8	619
R.6063.5	GD	Burns Bluff	6,7,8	141	18	290	0.1762	0.704916	0.704563	2.9	11.2	0.1563	0.512736	2.6	730
R.6057.16	TO	Burns Bluff	6,8	141	56	489	0.3342	0.707202	0.706532	3.3	21.5	0.0920	0.512454	-1.7	1105
R.6057.20	QDI	Burns Bluff	6,8	141	8	281	0.0816	0.704408	0.704245	1.6	5.5	0.1773	0.512832	4.1	589
R.6057.30	TO	Burns Bluff	6,8	141	36	718	0.1455	0.705706	0.705414	3.0	13.4	0.1373	0.512667	1.6	821
R.2793.1	GA	Moore Point	6,8	140	1	236	0.0130	0.704424	0.704399	0.3	0.9	0.2175	0.512875	4.3	576
R.5259.1	GA	Mount Eissenger	9	140	3	424	0.0188	0.705195	0.705157	1.5	4.5	0.2031	0.512750	2.1	781
R.6057.10	GA	Burns Bluff	6,8	141	29	296	0.2832	0.704958	0.704390	3.5	12.4	0.1727	0.512822	4.0	599
North-east Palmer Land															
E.4021.1	GD	Welch Mountains	4	124	85	415	0.5863	0.707420	0.706387	3.2	16.4	0.1163	0.512432	-2.7	1176
E.4012.1	GD	Black Coast	4	120	81	495	0.4750	0.706540	0.705730	3.7	21.5	0.1054	0.512424	-2.8	1176
R.1906.5	GD	Mount Charity	5	120	233	219	3.0858	0.711129	0.705866	6.7	24.2	0.1666	0.512432	-3.6	1237
R.1906.7	GD	Mount Charity	5	120	114	312	1.0612	0.707736	0.705926	5.2	17.7	0.1778	0.512472	-2.9	1190
R.4278.1	GA	Black Coast	4	120	12	532	0.0669	0.705137	0.705023	5.0	20.7	0.1473	0.512471	-2.5	1154
R.4280.2	GA	Black Coast	4	120	85	524	0.4692	0.705752	0.704952	3.2	13.6	0.1425	0.512515	-1.6	1079
E.4178.1	GD	Mount Jackson	4	114	45	455	0.2890	0.705220	0.704752	2.8	14.4	0.1165	0.512537	-0.8	1012
R.4230.1	GD	Black Coast	4	108	89	316	0.8153	0.707845	0.706594	3.3	17.7	0.1135	0.512346	-4.6	1305
E.4065.1	GD	Giannini Peak	4	105	155	367	1.2210	0.708389	0.706567	3.9	18.9	0.1261	0.512365	-4.4	1290
Late Jurassic (146-157)															
North-west Palmer Land															
R.5260.2	GA	Mount Eissenger	9	150	64	216	0.8605	0.707769	0.705934	1.8	7.6	0.1429	0.512635	1.0	886
R.5260.3	GR	Mount Eissenger	9	150	76	239	0.9216	0.708800	0.706835	7.1	37.6	0.1147	0.512448	-2.1	1146
Middle Jurassic (178-157)															
Graham Land															
R.312.2	GR	Bildad Peak	1	163	144	348	1.1943	0.709060	0.706293	6.4	35.4	0.1098	0.512404	-2.8	1204
R.326.2	GD	Mount Fritsche	1	164	76	311	0.7099	0.708450	0.706795	3.7	20.0	0.1112	0.512361	-3.6	1271
R.302.1	DI	Bildad Peak	1	167	108	744	0.4199	0.707180	0.706183	6.0	24.5	0.1479	0.512425	-3.1	1235
R.310.1	GD	Bildad Peak	1	167	172	291	1.7200	0.710140	0.706056	4.7	25.1	0.1121	0.512396	-2.9	1219
R.2605.1	GA	Scharer Bluff	1	175	18	378	0.1402	0.708330	0.707981	2.1	9.1	0.1407	0.512365	-4.1	1314
R.2605.2	GA	Scharer Bluff	1	175	74	303	0.7067	0.709950	0.708192	4.2	20.3	0.1244	0.512296	-5.1	1388
R.2606.1	GA	Scharer Bluff	1	175	46	366	0.3638	0.709930	0.709025	3.8	16.1	0.1418	0.512263	-6.1	1464
R.2606.6	GR	Scharer Bluff	1	175	243	249	2.8286	0.717200	0.710162	8.3	49.0	0.1025	0.512300	-4.5	1346
R.2607.4	MG	Scharer Bluff	1	175	265	131	5.8885	0.725070	0.710419	10.6	53.5	0.1197	0.512321	-4.5	1344
R.2624.1	GD	Trail Inlet	1	177	141	241	1.6861	0.711900	0.707657	6.2	32.2	0.1157	0.512356	-3.7	1285
R.2625.1	GD	Trail Inlet	1	177	140	276	1.4672	0.711160	0.707468	6.8	35.4	0.1162	0.512359	-3.6	1281
North-west Palmer Land															
R.6308.1	GD	Mount Ward	7	170	173	239	2.0899	0.713930	0.708879	10.0	52.7	0.1149	0.512213	-6.5	1492
R.6309.2	GD	Mount Ward	9	170	38	234	0.4647	0.708407	0.707284	2.9	14.2	0.1216	0.512398	-3.1	1232
R.6315.8	GR	Butler Peaks	7	170	190	27	20.7529	0.757891	0.707733	9.7	34.6	0.1698	0.512358	-4.9	1371
North-east Palmer Land															
R.1906.3	GR	Mount Charity	5	168	190	65	8.5040	0.728482	0.708170	5.7	25.2	0.1364	0.512381	-3.7	1282
R.1907.4	PO	Mount Charity	5	168	231	48	13.9566	0.740769	0.707434	6.9	23.7	0.1759	0.512496	-2.3	1173
R.1914.11	GR	Mount Charity	5	168	110	659	0.4852	0.709057	0.707898	5.2	31.0	0.1022	0.512242	-5.7	1431
Early Jurassic (208-178)															
Graham Land															
R.052.6	OGN	Roman Four	1	200	163	88	5.3428	0.721509	0.706314	10.5	53.4	0.1189	0.512421	-2.2	1189
R.321.3	GD	Target Hill	1	180	120	299	1.1647	0.709310	0.706329	4.5	28.2	0.0958	0.512359	-3.1	1244
R.2619.1	GA	M Pyramid	1	181	24	378	0.1837	0.707900	0.707427	2.7	12.6	0.1309	0.512361	-3.9	1304

Sample	Rock type	Locality		Age	Rb	Sr	$^{87}Rb/^{86}Sr$	$^{87}Sr/^{86}Sr$	$^{87}Sr/^{86}Sr_i$	Sm	Nd	$^{147}Sm/^{144}Nd$	$^{143}Nd/^{144}Nd$	εNd_i	T_{DM}
R.2619.2	GA	M Pyramid	1	181	26	367	0.2059	0.707870	0.707340	2.9	13.3	0.1327	0.512362	-3.9	1305
R.2619.4	GR	M Pyramid	1	181	153	952	0.4638	0.709450	0.708256	4.6	20.0	0.1404	0.512339	-4.5	1353
R.2620.2	GR	M Pyramid	1	181	270	163	4.7929	0.720460	0.708126	10.4	51.6	0.1214	0.512234	-6.1	1472
R.2612.3	GD	Pylon Point	1	204	175	596	0.8495	0.710040	0.707576	5.0	27.9	0.1088	0.512281	-4.7	1379
R.2612.5	GR	Pylon Point	1	204	406	143	8.2413	0.733280	0.709372	7.3	41.0	0.1075	0.512281	-4.6	1377
R.2614.1	GR	Curran Bluff	1	204	398	153	7.5515	0.734980	0.713073	20.9	127.0	0.0997	0.512193	-6.2	1489
R.2614.3	GR	Curran Bluff	1	204	357	173	5.9919	0.731200	0.713817	16.9	101.1	0.1011	0.512191	-6.2	1494
North-west Palmer Land															
R.5254.2	V	Mount Pitman	9	181	184	69	7.7705	0.725311	0.705313	10.8	49.4	0.1320	0.512424	-2.7	1210
R.5254.5	V	Mount Pitman	9	181	104	239	1.2557	0.712287	0.709056	8.3	42.2	0.1193	0.512406	-2.7	1215
R.5270.1	DI	Goettel Escarpment	7	182	46	382	0.3498	0.706802	0.705897	3.9	17.6	0.1331	0.512543	-0.4	1024
R.5271.4	GR	Goettel Escarpment	7	183	87	447	0.5668	0.707919	0.706444	11.8	64.1	0.1110	0.512471	-1.3	1097
R.2549.2	GD	Capella Rocks	9	203	36	990	0.1065	0.707215	0.706907	3.5	19.6	0.1081	0.512461	-1.2	1103
R.5280.2	GD	Campbell Ridges	7	203	131	310	1.2237	0.711610	0.708077	8.5	40.8	0.1261	0.512353	-3.7	1307
R.5280.4	PO	Campbell Ridges	9	203	134	94	4.1231	0.719044	0.707142	6.5	31.8	0.1234	0.512356	-3.6	1297
R.5504.2	GD	Auriga Nunataks	9	203	57	496	0.3324	0.707816	0.706856	2.0	21.1	0.0566	0.512394	-1.1	1101
North-east Palmer Land															
R.4908.11	GRG	Mount van Buren	4	206	360	66	15.7498	0.765920	0.719781	5.4	20.1	0.1630	0.512145	-8.7	1672
R.2109.2	GRG	Mount Jackson	4	199	330	80	11.9488	0.754753	0.720940	6.4	20.7	0.1853	0.512141	-9.4	1714
Triassic (248-206)															
Graham Land															
R.280.4	GR	Cole Peninsula	1	209	120	399	0.8640	0.709250	0.706682	6.4	37.6	0.1035	0.512391	-2.3	1202
R.5506.3	GRG	Elton Hill	9	210	186	39	13.8157	0.747093	0.705833	8.3	30.6	0.1647	0.512464	-2.5	1219
R.6157.1	GRG	Reluctant island	9	200	100	188	1.5359	0.710398	0.706030	9.0	54.0	0.1013	0.512382	-2.6	1214
R.5035.2	AM	N of Werner Peak	9	220	107	210	1.4675	0.713904	0.709312	4.1	16.3	0.1509	0.512197	-7.3	1583
R.5035.6	GR	N of Werner Peak	9	220	474	23	60.9030	0.898134	0.707575	0.7	2.6	0.1687	0.512273	-6.3	1512
North-west Palmer Land															
R.2479.1	GR	Mount Lepus	9	210	82	343	0.6886	0.707860	0.705803	4.2	23.9	0.1069	0.512494	-0.4	1045
R.2480.1	GD	Mount Lepus	7	210	75	555	0.3911	0.707090	0.705922	6.4	31.7	0.1220	0.512520	-0.3	1037
R.3239.4	OGN	Campbell Ridges	9	227	180	482	1.0827	0.712220	0.708724	5.1	24.5	0.1266	0.512254	-5.5	1453
R.5294.1	OGN	Sirius Cliffs	9	227	120	870	0.3986	0.706207	0.704920	9.5	41.0	0.1406	0.512338	-4.2	1361
R.5278.8	OGN	Campbell Ridges	7	227	139	608	0.6636	0.709655	0.707513	5.0	25.1	0.1216	0.512338	-3.7	1319
R.5297.3	PGN	Mount Lepus	7	210	121	316	1.1052	0.715572	0.712256	6.9	34.8	0.1202	0.512347	-3.6	1304
R.2436.2	PGN	Auriga Nunataks	9	227	188	443	1.2270	0.717259	0.713297	8.5	45.5	0.1124	0.512096	-8.1	1645
R.2535.6	OGN	Fomalhaut Nuns.	9	227	114	274	1.2002	0.715872	0.711997	2.6	16.0	0.0965	0.512192	-5.8	1478
R.2535.7	OGN	Fomalhaut Nuns.	9	227	124	271	1.3198	0.716208	0.711947	5.7	35.6	0.0973	0.512207	-5.5	1458
R.5257.1	OGN	Mount Eissenger	7	227	174	189	2.6741	0.724902	0.716268	0.8	3.7	0.1352	0.512543	-0.1	1030
R.5257.2	OGN	Mount Eissenger	9	227	81	190	1.2250	0.720105	0.716150	13.0	62.9	0.1253	0.512548	0.3	997
North-east Palmer Land															
R.1905.1	DI	Mount Charity	5	232	150	770	0.5628	0.708320	0.706463	7.7	35.5	0.1305	0.512361	-3.4	1305
R.1905.4	GR	Mount Charity	5	232	185	489	1.0911	0.710352	0.706752	6.2	49.3	0.0767	0.512278	-3.5	1307
R.1905.5	GR	Mount Charity	5	232	245	117	6.0764	0.726115	0.706064	1.2	3.9	0.1799	0.512550	-1.2	1128
R.1907.2	GR	Mount Charity	5	232	242	113	6.2259	0.726957	0.706413	1.6	4.6	0.2116	0.512503	-3.1	1276
R.4552.2	OGN	Mount Nordhill	4	220	176	150	3.4004	0.726175	0.715536	8.9	43.3	0.1248	0.512143	-7.6	1605
R.4552.9	GGN	Mount Nordhill	4	220	308	109	8.2244	0.742662	0.716929	6.8	34.5	0.1201	0.512126	-7.8	1619
R.4920.5	GR	Mount Nordhill	9	220	201	253	2.3031	0.716426	0.709220	16.3	81.5	0.1208	0.512121	-8.0	1628
R.4920.12	GR	Mount Nordhill	4	220	289	224	3.7368	0.724185	0.712493	8.3	40.2	0.1255	0.512170	-7.1	1570
R.4922.1	MY	Steele Peak	9	220	125	448	0.8060	0.707357	0.704835	2.7	14.4	0.1138	0.512531	0.2	998
R.4942.4	GD	Hall Ridge	4	211	77	477	0.4689	0.706893	0.705486	4.9	22.9	0.1286	0.512453	-1.8	1159
R.5006.7	GD	Pinther Ridge	4	209	95	465	0.5911	0.707586	0.705829	8.6	46.0	0.1128	0.512355	-3.3	1277

Sample	Rock type	Locality		Age	Rb	Sr	$^{87}Rb/^{86}Sr$	$^{87}Sr/^{86}Sr$	$^{87}Sr/^{86}Sr_i$	Sm	Nd	$^{147}Sm/^{144}Nd$	$^{143}Nd/^{144}Nd$	εNd_i	T_{DM}
Pre-Triassic															
Graham Land															
BR.041.1	SH	Latille Island	9	250	139	393	1.0244	0.712480	0.708837	5.8	29.5	0.1195	0.512293	-4.3	1380
BR.072.1	SST	Hope Bay	1	250	72	371	0.5581	0.709500	0.707515	6.8	30.8	0.1336	0.512356	-3.5	1320
BR.072.2	SST	Hope Bay	1	250	95	361	0.7574	0.709500	0.706807	5.1	28.7	0.1074	0.512341	-2.9	1278
BR.072.3	SST	Hope Bay	1	250	204	138	4.3041	0.723320	0.708013	7.2	35.8	0.1212	0.512301	-4.2	1372
R.3415.14	PG	Target Hill	2	321	45	211	0.6137	0.708036	0.705232	1.3	2.9	0.2603	0.512703	-1.3	1200
R.3632.1	GR	Marsh Spur	3	325	111	211	1.5168	0.713053	0.706037	9.9	79.5	0.0753	0.512324	-1.1	1183
R.3632.2	GR	Marsh Spur	3	325	136	68	5.7731	0.732655	0.705951	5.7	25.8	0.1336	0.512413	-1.8	1238
R.3632.4	GR	Marsh Spur	3	325	153	36	12.2990	0.763040	0.706149	2.6	7.8	0.2031	0.512602	-1.0	1173
R.3899.18	GR	Mount Lagado	3	325	135	114	3.4434	0.719880	0.703952	1.7	4.9	0.2089	0.512550	-2.2	1274
R.3900.3	GR	Mount Lagado	3	325	62	262	0.6959	0.707110	0.703891	0.6	1.2	0.2994	0.512867	0.2	1076
R.3431.1	GGN	Leppard Glacier	3	392	139	232	1.7426	0.714041	0.704314	3.0	19.9	0.0928	0.512495	2.4	932
R.3431.5	GGN	Leppard Glacier	3	392	74	273	0.7796	0.707910	0.703559	1.5	6.2	0.1444	0.512455	-1.0	1219
R.3431.17	AM	Leppard Glacier	3	392	39	201	0.5606	0.706805	0.703676	2.7	9.0	0.1829	0.512802	3.9	796
R.3434.1	GGN	Leppard Glacier	3	392	118	229	1.4976	0.713111	0.704752	3.2	18.4	0.1043	0.512465	1.3	1034
R.3434.2	GGN	Leppard Glacier	3	392	63	171	1.0656	0.709121	0.703173	1.7	5.8	0.1734	0.512566	-0.2	1161
R.3434.6	GGN	Leppard Glacier	2	392	71	272	0.7551	0.707325	0.703110	4.0	18.6	0.1289	0.512519	1.1	1050
R.3434.7	GGN	Leppard Glacier	3	392	122	183	1.9257	0.715614	0.704865	3.3	19.0	0.1047	0.512478	1.5	1014
R.4016.5	AM	Leppard Glacier	3	392	61	211	0.8382	0.708063	0.703384	7.3	28.9	0.1529	0.512652	2.5	927
R.5511.1	OGN	Target Hill	9	392	39	199	0.5718	0.708604	0.705412	3.0	17.5	0.1031	0.512521	2.4	933
R.348.1A	GN	Adie Inlet	1	246	174	229	2.1962	0.722770	0.715085	8.1	38.8	0.1255	0.512158	-7.1	1588
R.348.1B	GN	Adie Inlet	1	246	148	276	1.5580	0.720930	0.715478	5.4	25.7	0.1270	0.512181	-6.7	1560
R.348.2	GN	Adie Inlet	1	246	151	256	1.7089	0.721100	0.715120	6.0	28.0	0.1283	0.512182	-6.8	1561
R.349.1	GN	Adie Inlet	1	246	125	206	1.7474	0.719760	0.713645	8.4	40.9	0.1236	0.512179	-6.7	1555
R.349.2	GN	Adie Inlet	1	246	129	200	1.8724	0.720190	0.713638	8.2	39.1	0.1268	0.512186	-6.6	1552
R.349.3	AM	Adie Inlet	1	246	99	188	1.5214	0.720560	0.715236	7.1	**33.8**	0.1277	0.512104	-8.3	1667
R.346.5	AM	Adie Inlet	1	246	39	218	0.5170	0.707650	0.705841	2.1	7.2	0.1781	0.512319	-5.6	1481
R.350.1	AM	Adie Inlet	1	246	87	796	0.3274	0.707460	0.706314	8.3	38.7	0.1295	0.512338	-3.7	1338
North-east Palmer Land															
R.4293.2	PGN	Solem Ridge	4	220	257	102	7.3091	0.745647	0.722777	10.4	50.59	0.1240	0.512067	-9.1	1707
R.4294.1	PGN	Mount Nordhill	4	220	144	177	2.3546	0.733153	0.725786	3.4	17.50	0.1161	0.512050	-9.2	1714
R.4920.8	PGN	Mount Nordhill	4	220	140	216	1.8817	0.731113	0.725226	10.9	54.70	0.1200	0.512035	-9.6	1742

Complete Sr and Nd isotope data set for granitoids and country rocks. Published data are reproduced here, in order to correct errors in original papers and theses, and because in some cases revised ages are used for recalculations. Rock types: AM amphibolite; DI diorite; GA gabbro; GD granodiorite; GGN granite gneiss; GR granite; MG metagranite; MY mylonite; OGN orthogneiss; PG pegmatite; PGN paragneiss; PO porphyry; QDI quartz diorite; SST sandstone; TO tonalite; V unclassified volcanic rocks.

References

1. HOLE, M.J. 1986. Time controlled geochemistry of igneous rocks of the Antarctic Peninsula. Unpublished PhD thesis, University of London.
2. MILNE, A.J. & MILLAR, I.L. 1989. The significance of mid-Palaeozoic basement in Graham Land, Antarctic Peninsula. *Journal of the Geological Society, London*, **146**, 207-210.
3. MILNE, A.J. 1990. The pre-Mesozoic geological evolution of Graham Land, Antarctica. Unpublished PhD thesis, Open University.
4. WEVER, H.E., MILLAR, I.L. & PANKHURST, R.J. 1994. Geochronology and radiogenic isotope geology of Mesozoic rocks from eastern Palmer Land, Antarctic Peninsula: crustal anatexis in arc-related granitoid genesis. *Journal of South American Earth Sciences*, **7**, 69-83.
5. SCARROW, J.H., PANKHURST, R.J., LEAT, P.T. & VAUGHAN, A.P.M. 1996. Antarctic Peninsula granitoid petrogenesis: a case study from Mount Charity, north-eastern Palmer Land. *Antarctic Science*, **8(2)**, 193-206.

6. VAUGHAN, A.P.M., WAREHAM, C.D. & MILLAR, I.L., 1997. Granitoid pluton formation by spreading of continental crust: the Wiley Glacier complex, northwest Palmer Land, Antarctica. *Tectonophysics*, **283**, 35-60.
7. WAREHAM, C.D., MILLAR, I.L. & VAUGHAN, A.P.M. 1997a. The generation of sodic granite magmas, western Palmer Land, Antarctic Peninsula. *Contributions to Mineralogy and Petrology*, **128**, 81-96.
8. WAREHAM, C.D., VAUGHAN, A.P.M. & MILLAR, I.L. 1997b. The Wiley Glacier complex, Antarctic Peninsula: pluton growth by pulsing of granitoid magmas. *Chemical Geology*, **143**, 65-80.
9. This paper.

Table 1. Pb isotope data for leached feldspars from Antarctic Peninsula granitoids.

Sample	Rock type	Locality	Mineral	Age (Ma)	$^{206}Pb/^{204}Pb$	$^{207}Pb/^{204}Pb$	$^{208}Pb/^{204}Pb$
Graham Land							
BR.024.4	diorite	Faure Islands	Pl	48	18.729	15.621	38.492
R.080.1	granite	Horseshoe Island	Pl	67	18.796	15.634	38.566
R.312.2	granite	Bildad Peak	Pl	163	18.569	15.658	38.441
R.326.2	granodiorite	Mount Fritsche	Pl	164	18.640	15.649	38.510
R.2614.1	2-mica granite	Curran Bluff	Pl	204	18.735	15.664	38.695
R.349.1	granodiorite gneiss	Adie Inlet	Pl	?550	18.566	15.668	38.460
R.3632.2	metagranite	Marsh Spur	Pl	325	18.468	15.616	38.164
R.5511.1	gneiss	Target Hill	Pl	392	18.985	15.660	38.535
NW Palmer Land							
R.5256.1	granite	Mount Pitman	Pl	60	18.751	15.616	38.504
R.5736.1	granodiorite	Scorpio Peaks	Kfs	70	18.725	15.609	38.452
R.5796.4	granodiorite	Cetus Hill	Pl	120	18.757	15.636	38.522
R.3216.3	tonalite	Burns Bluff	Pl	140	18.701	15.658	38.546
R.5284.1	granodiorite	Renner Peak	Pl	140	18.683	15.633	38.483
R.6057.10	gabbro	Burns Bluff	Pl	141	18.571	15.623	38.370
R.5287.1	diorite	Creswick Peaks	Pl	141	18.681	15.637	38.508
R.5270.1	diorite	Goettel Escarpment	Pl	182	18.644	15.646	38.463
R.5271.4	foliated granite	Goettel Escarpment	Kfs	183	18.641	15.647	38.476
R.5504.2	foliated granodiorite	Auriga Nunataks	Kfs	203	18.741	15.650	38.543
R.5278.8	granite gneiss	Campbell Ridges	Kfs	227	18.707	15.654	38.604
NE Palmer Land							
R.4908.10	leucogranite gneiss	Mount van Buren	Pl	206	18.679	15.655	38.446
R.5006.7	metagranodiorite	Pinther Ridge	Pl	209	18.669	15.657	38.532
R.4942.4	metagranodiorite	Hall Ridge	Pl	211	18.802	15.662	38.626
R.4552.9	leucogranite gneiss	Mount Nordhill	Pl	220	18.715	15.661	38.512
R.4920.12	megacrystic granite	Mount Nordhill	Pl	220	18.694	15.672	38.545

Pl – plagioclase; Kfs – K-Feldspar.

Table 2.
O-isotope composition of granitoids from the Ellsworth-Whitmore Mountains crustal block.

			$\delta^{18}O_{SMOW}$		
Sample	**Rock type**	**Locality**	**Whole-rock**	**Quartz**	**Plagioclase**
R.2243.4	granite	Pirrit Hills	9.1	10.0	9.0
R.2226.4	granite	Linck Nunatak	10.0		
R.2215.4	granite	Pagano Nunatak	10.1	11.7	9.9